Quantum hall criticality and localization in graphene with short-range impurities at the Dirac point

Quantum Hall Criticality and Localization in Graphene with Short-Range Impurities at the Dirac Point

S. Gattenlöhner,[1] W.-R. Hannes,[1] P. M. Ostrovsky,[2,3] I. V. Gornyi,[4,5] A. D. Mirlin,[4,6,7] and M. Titov[8]
[1]School of Engineering and Physical Sciences, Heriot-Watt University, Edinburgh EH14 4AS, United Kingdom
[2]Max-Planck-Institut für Festkörperforschung, Heisenbergstr. 1, 70569, Stuttgart, Germany
[3]L. D. Landau Institute for Theoretical Physics RAS, 119334 Moscow, Russia
[4]Institut für Nanotechnologie, Karlsruhe Institute of Technology, 76021 Karlsruhe, Germany
[5]A. F. Ioffe Physico-Technical Institute, 194021 St. Petersburg, Russia
[6]Institut für Theorie der kondensierten Materie and DFG Center for Functional Nanostructures, Karlsruhe Institute of Technology, 76128 Karlsruhe, Germany
[7]Petersburg Nuclear Physics Institute, 188300 St. Petersburg, Russia
[8] Radboud University Nijmegen, Institute for Molecules and Materials, NL-6525 AJ Nijmegen, Netherlands
(Received 25 June 2013; published 14 January 2014)

We explore the longitudinal conductivity of graphene at the Dirac point in a strong magnetic field with two types of short-range scatterers: adatoms that mix the valleys and "scalar" impurities that do not mix them. A scattering theory for the Dirac equation is employed to express the conductance of a graphene sample as a function of impurity coordinates; an averaging over impurity positions is then performed numerically. The conductivity σ is equal to the ballistic value $4e^2/\pi h$ for each disorder realization, provided the number of flux quanta considerably exceeds the number of impurities. For weaker fields, the conductivity in the presence of scalar impurities scales to the quantum-Hall critical point with $\sigma \simeq 4 \times 0.4e^2/h$ at half filling or to zero away from half filling due to the onset of Anderson localization. For adatoms, the localization behavior is also obtained at half filling due to splitting of the critical energy by intervalley scattering. Our results reveal a complex scaling flow governed by fixed points of different symmetry classes: remarkably, all key manifestations of Anderson localization and criticality in two dimensions are observed numerically in a single setup.

DOI: 10.1103/PhysRevLett.112.026802 PACS numbers: 72.80.Vp, 73.22.-f, 73.63.-b

The discovery of graphene has initiated an intense study of its electronic properties [1,2]. From the fundamental point of view, the interest to graphene is largely motivated by the quasirelativistic character of its spectrum: charge carriers in graphene are two-dimensional (2D) massless Dirac fermions. This leads to a variety of remarkable phenomena governed by the inherent topology of Dirac fermions as well as by their physics in the presence of various types of disorder and interactions.

Controllable functionalization of the graphene surface is possible by a variety of tools, including hydrogenation [3–6], fluorination [7], adsorption of gas molecules [8,9], ion irradiation [10,11], electron-beam irradiation [12], and deposition of metallic islands [13]. Adatoms, deposited molecules or islands, and defects engineered in this way serve as strong short-range scatterers as has been also supported by a density functional theory analysis [14]. Furthermore, such scatterers also exist in pristine graphene and may dominate its transport properties (in particular, in suspended devices [15,16]). Thus, it is important to theoretically explore the transport in graphene with this kind of disorder. Away from the Dirac point, the conductivity of such structures is sufficiently well understood [17–23].

Electronic transport properties of graphene near zero energy (Dirac point) are particularly exciting. Remarkably, experiments discovered [24,25] that the conductivity of graphene at the Dirac point is essentially independent of temperature in a broad range (from 300 K down to 30 mK) and has a value close to the conductance quantum e^2/h (times four, which is the total spin and valley degeneracy). This discovery attracted a great interest because in conventional materials, once the conductivity is close to e^2/h, it becomes strongly suppressed by Anderson localization with lowering temperature. The above experiments, thus, indicate that the Dirac-point physics of disordered graphene may be controlled by the vicinity of some quantum critical point. Indeed, theoretical investigations have shown that for certain classes of disorder that preserve some of symmetries of the clean Dirac Hamiltonian, the system avoids Anderson localization [17,26,27]. Recent work [28] demonstrated the feasibility of the systematic experimental study of localization near the Dirac point.

A quantizing magnetic field yields a further remarkable twist to the fascinating physics of graphene near the Dirac point. The Dirac character of the spectrum makes graphene a unique example of a system where the quantum Hall (QH) effect can be observed up to the room temperature [29]. The zeroth Landau level in graphene, with half of its edge branches being electronlike and the other half holelike [30,31], has no analogue in semiconducting 2D electron

systems with parabolic dispersion. Recent works on graphene in a strong magnetic field show fractional QH effect as well as an insulating behavior at the Dirac point, indicating a splitting of the critical energy in the zeroth Landau level [32–35].

The goal of this Letter is to study the Dirac-point conduction of graphene with randomly positioned strong short-range impurities in a quantizing transverse magnetic field. An analytical theory of transport in graphene developed in Refs. [17,26,27,36] maps the problem onto a field theory—nonlinear σ model (NLσM)—that is subsequently analyzed by renormalization group means. The crucial role in this analysis is played by the symmetry class and the topology of the NLσM. These field theories possess in 2D a rich family of nontrivial fixed points. Scaling flow between these fixed points governs the evolution of conductivity with increasing system size or decreasing temperature.

It is important to stress, however, that the NLσM is fully controllable at conductivity $\sigma \gg e^2/h$, while the physics near zero energy and the corresponding fixed points correspond to $\sigma \sim e^2/h$ (strong coupling for the field theory). Thus, an extrapolation of the theory is required. While this is a common ideology in condensed matter physics, one cannot, *a priori*, exclude the possibility of a more complex behavior not anticipated from the weak coupling expansion. Thus, a numerical modeling is of paramount importance to probe the strong-coupling physics. In addition to verifying qualitative predictions of the NLσM, such a modeling should give values of conductivity at fixed points and quantitatively characterize crossovers between them. A number of works have studied transport and localization in graphene with scatterers near the Dirac point [23,37–39] by numerical analysis of the Kubo conductivity or of wave packet propagation. The results for disorder formed by a low concentration of vacancies [23,38,39] disagree with expectations based on NLσM that the chiral symmetry inhibits localization.

In this Letter, we use the unfolded scattering theory [40–42] for the Dirac Hamiltonian with pointlike scatterers and extend it to incorporate magnetic fields. This allows us to get an exact expression for the conductivity for a given configuration of impurities. Subsequent averaging over impurity positions is performed numerically. This combination of analytical and numerical tools turns out to be a very efficient way of evaluating the conductivity of graphene with rare short-range scatterers.

We consider two types of impurities: (i) "scalar" impurities represented by a smooth electrostatic potential that does not mix the graphene valleys and (ii) adatoms represented by an on-site impurity potential mixing the valleys. Our results yield a rich scaling flow controlled by a number of fixed points of different symmetry classes, in qualitative agreement with predictions based on the σ model. We also demonstrate that in the limit of high magnetic field such that the number of flux quanta piercing the sample exceeds the number of impurities, the conductivity returns to its ballistic value, $\sigma_{xx} \approx 4e^2/\pi h$, for each disorder realization.

Electronic properties of clean graphene are modeled by the Dirac Hamiltonian, $H_A = v\boldsymbol{\sigma}(\boldsymbol{p} - e\boldsymbol{A}/c)$, where $\boldsymbol{\sigma} = (\sigma_x, \sigma_y)$, $\boldsymbol{p}$ is the 2D momentum operator, $\boldsymbol{A}$ is the vector potential, and $v \approx 10^6$ m/s is the electron velocity. The disorder potential is given by a superposition of individual impurity potentials. The distance between impurities is assumed to be much larger than both the lattice constant and the spatial range of an impurity.

We consider a rectangular graphene sample with periodic boundary conditions in the y direction ($0 < y < W$) and open boundary conditions in the x direction ($0 < x < L$). The latter correspond to highly doped graphene leads [40,43]. The transport properties of this setup are described by a generating function [40–42,44], $\mathcal{F}(\phi)$, whose derivatives with respect to the fictitious source field ϕ are related to the moments of the transmission distribution. In particular, Landauer's formula for the conductance G can be written as $\mathrm{G} = (4e^2/h)\partial^2\mathcal{F}/\partial\phi^2|_{\phi=0}$. Within the "unfolded scattering theory" [40,41], the impurity contribution to $\mathcal{F}(\phi)$ is expressed in terms of Green functions $G_A(\boldsymbol{r}_m, \boldsymbol{r}_n; \phi)$ of the clean system connecting impurity positions and the matrix $\hat{T} = \mathrm{diag}(T_1, T_2, \ldots, T_N)$ constructed from individual impurity T matrices in the s-wave approximation at zero energy; see the Supplemental Material [45] for details.

A remarkable feature of the zero-energy state of clean graphene is the existence of a nonunitary gauge transformation, making it possible to gauge away the entire magnetic field [44]. This transformation can be formulated as

$$G_A(\boldsymbol{r}, \boldsymbol{r}') = e^{\chi(\boldsymbol{r})\sigma_z + i\varphi(\boldsymbol{r})} G_0(\boldsymbol{r}, \boldsymbol{r}') e^{\chi(\boldsymbol{r}')\sigma_z - i\varphi(\boldsymbol{r}')}, \qquad (1)$$

where G_0 refers to the zero-energy Green function associated with the Hamiltonian $H_0 = v\boldsymbol{\sigma}\boldsymbol{p}$. The phases $\varphi(\boldsymbol{r})$ and $\chi(\boldsymbol{r})$ satisfy $\partial_x\varphi + \partial_y\chi = eA_x/c\hbar$ and $\partial_y\varphi - \partial_x\chi = eA_y/c\hbar$. In the Landau gauge, $\boldsymbol{A} = (0, Bx + \phi c/2eL)$, and fixing φ and χ by the requirement $\chi(0) = \chi(L) = 0$ (ensuring that the boundary conditions at the graphene-lead interfaces are not affected by the magnetic field), we find

$$\chi(\boldsymbol{r}) = x(L - x)/2\ell_B^2, \quad \varphi(\boldsymbol{r}) = y(L/2\ell_B^2 + \phi/2L), \quad (2)$$

where $\ell_B = (c\hbar/eB)^{1/2}$ is the magnetic length.

Scalar impurities are described by the T matrix $T = 2\pi\ell_s$, where ℓ_s is a finite scattering length. Adatoms are characterized by a T matrix $T_\zeta^c = \ell_a(1 + \zeta\sigma_z\tau_z + \sigma_{-\zeta}\tau_- \exp[i\theta_\zeta^c] + \sigma_\zeta\tau_+ \exp[-i\theta_\zeta^c])$ that depends on the sublattice index ($\zeta = 1$ for the A and $\zeta = -1$ for the B sublattice) and a site "color" $c = -1, 0, 1$, encoding the Bloch phase at the impurity site. We use $\sigma_\pm = (\sigma_x \pm i\sigma_y)/\sqrt{2}$ and $\tau_\pm = (\tau_x \pm i\tau_y)/\sqrt{2}$ with $\sigma_{x,y,z}$ and

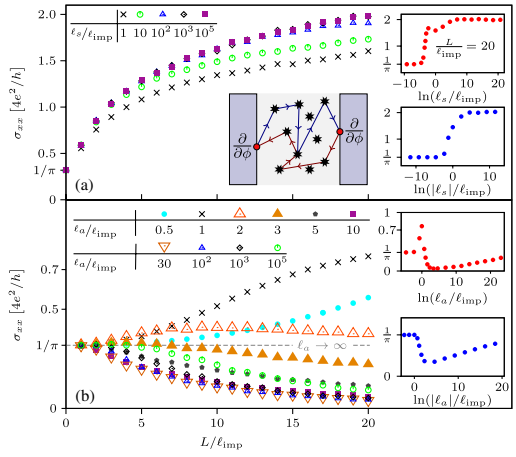

FIG. 1 (color online). Dirac-point conductivity of graphene with (a) scalar impurities and (b) adatoms in zero magnetic field as a function of the system size L. Insets show the dependence of σ_{xx} on the impurity strength ℓ_a and ℓ_s for a fixed system size $L = 20\ell_{\rm imp}$. In the upper insets all impurities have the same sign while in the lower insets the sign of the impurity potential is random. The sketch in (a) shows a typical path contributing to the conductance correction; this closed path connects the left with the right lead along impurity sites (★) which are characterized by their individual T matrices.

$\tau_{x,y,z}$ being the Pauli matrices in the sublattice and valley space, respectively. The phase $\theta^c_\pm = \pm\alpha + 4\pi c/3$ depends in addition on the angle α between the x axis and the bond direction of the graphene lattice.

In the wide-sample limit, $W \gg L$, we arrive at a general expression [45] for the conductance of the form

$$\mathrm{G} = \frac{4e^2}{h}\frac{\partial^2 \mathcal{F}}{\partial \phi^2}\bigg|_{\phi=0} = \frac{4e^2}{\pi h}(W/L + \pi S), \tag{3}$$

where S can be interpreted as the sum of amplitudes corresponding to closed paths via impurity sites that go from the left lead to the right one and then back to the left lead (see Fig. 1). The amplitudes are given by products of free Green functions describing the propagation between impurities and T matrices characterizing the scattering off each impurity. For scalar impurities, we find

$$S = 4\mathrm{Tr}(\hat{Y}_s^\dagger M_+ \hat{Y}_s M_- - \hat{Y}^2 M_+ M_-), \tag{4}$$

where $\hat{Y} = L^{-1}\mathrm{diag}(y_1, y_2, \ldots, y_N)$ is the diagonal matrix consisting of y components of the impurity coordinates, $\hat{Y}_s = \hat{Y} + i\ell_s\sigma_y/2L$, and $M_\pm = (1 \pm i\pi\ell_s\hat{R}/2L)^{-1}$. The elements of the matrix $\hat{R}$ are given by

$$R_{nm} = e^{\chi(\boldsymbol{r}_n)\sigma_z}\begin{pmatrix} \frac{1}{\sin(z_n+z_m^*)} & \frac{1-\delta_{mn}}{\sin(z_n-z_m)} \\ \frac{1-\delta_{mn}}{\sin(z_n^*-z_m^*)} & \frac{1}{\sin(z_n^*+z_m)} \end{pmatrix} e^{\chi(\boldsymbol{r}_m)\sigma_z}, \tag{5}$$

where $z_n = \pi(x_n + iy_n)/2L$ and δ_{nm} is the Kronecker symbol. Thus, the calculation of the conductance for a particular configuration of scalar impurities amounts to the inversion of a matrix of the size $2N \times 2N$. In the case of adatoms, S has a similar structure [45].

The longitudinal conductivity is defined as $\sigma_{xx} = LG/W$, where $W \gg L$. For the numerical analysis, we fix $W = 4L$ and plot σ_{xx} as a function of the system size L, while keeping the magnetic length ℓ_B and the average distance between impurities $\ell_{\rm imp}$ fixed.

We begin the presentation of our results by briefly considering the regime of zero magnetic field. Figure 1 displays the conductivity of graphene with scalar impurities and adatoms for various impurity strengths. The case of scalar impurities is shown in Fig. 1(a). In the limit $\ell_s/\ell_{\rm imp} \to \infty$, the system belongs to the class DIII (with a Wess-Zumino term) and shows a logarithmic scaling towards a "supermetal" (infinite-conductivity) fixed point [41]. A finite value of ℓ_s breaks the chiral symmetry, thus, yielding the symmetry class AII (with a topological θ term). However, the supermetallic behavior remains almost unchanged [27].

A crossover due to symmetry breaking also takes place for the case of adatoms in Fig. 1(b), but the behavior of the conductivity is essentially different. As expected, Anderson localization sets in at long scales since the system belongs to the conventional Wigner-Dyson symmetry class AI. For a fixed concentration of impurities, $\ell_{\rm imp}^{-2}$, the localization length is a nonmonotonic function of the impurity strength parametrized by the scattering length ℓ_a. Indeed, in the limit $\ell_a \ll \ell_{\rm imp}$, the mean free path is large, so that the system remains ballistic up to large distances. The opposite limit, $\ell_a/\ell_{\rm imp} \to \infty$, corresponds to the case of vacancies that preserve a chiral symmetry of the Hamiltonian. The system in this case belongs to the chiral class BDI and its conductivity remains finite (no localization) in the limit $L \to \infty$ [41]. Thus, there exists an intermediate value of the ratio $\ell_a/\ell_{\rm imp}$ for which the localization is the strongest. For large (but finite) values of $\ell_a/\ell_{\rm imp}$, the system behaves as chiral up to a certain scale due to the vicinity to a fixed point of class BDI, and then gets attracted by the localization fixed point of class AI. We choose $\ell_a/\ell_{\rm imp} = 50$ to illustrate the behavior of the system in magnetic field.

While our results showing that the localization exists for a generic disorder but disappears in the chiral limit (zero energy and $\ell_a/\ell_{\rm imp} \to \infty$) are consistent with NL$\sigma$M, they are at variance with numerical works [23,38,39]. Apparently, numerical approaches used in these papers were not sufficient to reliably explore quantum interference effects at the Dirac point.

We are now in a position to turn to the case of strong magnetic field. Our main results are shown in Fig. 2. For scalar impurities of random sign, the center of the zeroth Landau level remains at the Dirac point, $E = 0$, where the

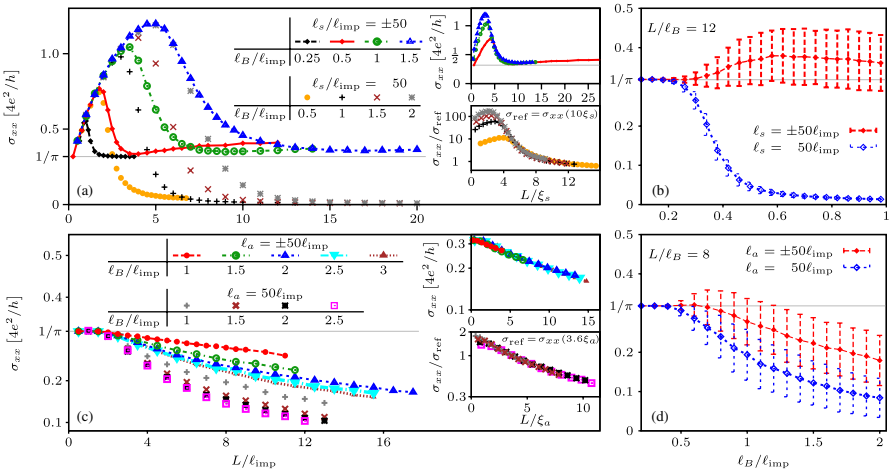

FIG. 2 (color online). Zero-energy conductivity σ_{xx} of graphene with scalar impurities (a),(b) and adatoms (c),(d). Left panels: evolution of σ_{xx} with length L for different values of the ratio $\ell_B/\ell_{\rm imp}$ of the magnetic length to the distance between impurities. The symmetry breaking pattern is DIII → AII → A for weaker B and DIII → AIII → A for stronger B in panel (a) and BDI → AI → A for weaker B and BDI → AIII → A for stronger B in panel (c). Scaling flow towards the QH critical point in (a) and localization in (a),(c) is shown in the insets by rescaling of the curves to a length ξ_s (respectively, ξ_a). For the considered range of parameters, the obtained values of ξ_s and ξ_a are well approximated by phenomenological expressions $\xi_s = 1.17\ell_B(1 + 0.126\ell_{\rm imp}/\ell_B)$ and $\xi_a = \ell_{\rm imp} + 8.85\exp(-1.73\ell_B/\ell_{\rm imp})$. For impurities of the same sign, an additional rescaling of σ_{xx} reflects the two-parameter scaling in magnetic field for $\theta \neq 0, \pi$. Right panels: σ_{xx} as a function of $\ell_B/\ell_{\rm imp}$ for fixed large L/ℓ_B. For moderately strong B the system is either at QH criticality or gets localized. For stronger B, a quasiballistic transport regime with $\sigma = 4e^2/\pi h$ emerges. Vertical bars show mesoscopic fluctuations.

conductivity is calculated. Different curves correspond to different strengths of the magnetic field B parametrized by ℓ_B. For small system sizes L, all curves follow the same supermetallic scaling (class AII) characteristic for the zero-B case. When the magnetic field becomes important, the symmetry class changes. While for infinitely strong impurities this would be the chiral class AIII with the Wess-Zumino term, the finite value of ℓ_s places the system into the class A with a $\theta = \pi$ topological term [36]. This implies that the system should flow into the QH critical point, see upper inset in Fig. 2(a). The obtained value of the QH critical conductivity is $\sigma_* \simeq 4 \times 0.4e^2/h$, where the factor four is the total (spin and valley) degeneracy of the scalar-impurity model. Remarkably, this critical value is approached from the bottom. This value is close to the one obtained recently in Ref. [46] for a tight-binding model of graphene with box disorder at all sites. Evidence of quantum Hall criticality of Dirac fermions with long-range disorder was also reported in Ref. [47] where the Thouless number was numerically evaluated.

When all impurities are of the same sign, the critical state of the lowest Landau level is shifted from the zero-energy point. In terms of the NLσM theory this implies that the topological term has now a prefactor θ different from π. The system should then scale towards $\sigma = 0$ due to Anderson localization. This is indeed seen in Fig. 2(a) (the main panel and lower inset). It is worth emphasizing that this localization in the QH regime is much more efficient than that in zero B (see Fig. 1).

Figure 2(b) demonstrates another peculiarity of the problem. When the magnetic field is sufficiently strong such that the number of flux quanta N_Φ exceeds $4N$ where N is the number of impurities, the conductivity is given by its ballistic value $\sigma_{xx} = 4e^2/\pi h$ independent of the impurity positions. The condition $N_\Phi > 4N$, which translates into $\ell_B < \ell_{\rm imp}/2\sqrt{2\pi}$, can be understood from the following argument. Each pointlike scalar impurity cannot broaden the entire Landau level but rather reduces its degeneracy by splitting four levels [48]. Indeed, the wave functions of the degenerate Landau level can be superimposed such that their values at the impurity sites are zero. Thus, for $N < N_\Phi/4$, a macroscopic degeneracy of the Landau level remains, with the corresponding eigenstates unaffected by the impurities. As a result, the system does not flow to either QH or localization fixed points but rather stays essentially ballistic. When $N \ll N_\Phi$, we obtain the "ballistic conductivity" $\sigma = 4e^2/\pi h$ with exponentially suppressed fluctuations.

Figures 2(c) and 2(d) show the behavior of the conductivity in the presence of adatoms. The limit of infinitely strong adatoms (i.e., vacancies, $\ell_a \to \infty$) would correspond to the chiral symmetry class AIII, which is characterized by a constant value of σ_{xx} close to $(4/\pi)e^2/h$. This is what we indeed observe at not too large L in Fig. 2(c). For larger L the chiral symmetry breaking due to a finite ℓ_a occurs, and the system is in the symmetry class A with a topological term. Contrary to the case of scalar impurities, we observe localization (i.e., $\theta \neq \pi$) both for symmetric and

asymmetric distribution of random potential. This is because the intervalley scattering splits the critical state of the lowest Landau level [36], implying that the states at $E = 0$ are now localized.

Similar to the model with scalar impurities, in a strong magnetic field we observe the ballistic value of conductivity $\sigma = (4/\pi)e^2/h$ with no conductance fluctuations, as is seen in Fig. 2(d). For adatoms, the condition that a part of the Landau level eigenstates remain unaffected reads $N < N_\Phi$, or equivalently, $\ell_B/\ell_{\rm imp} < 1/\sqrt{2\pi}$.

To summarize, we have studied the zero-energy conductivity of graphene with strong (but not infinitely strong) short-range impurities in a magnetic field. For this purpose, we have employed the unfolded scattering theory for the Dirac Hamiltonian with pointlike scatterers. The problem shows a complex scaling behavior controlled by a number of fixed points reflecting the (approximate and exact) symmetries as well as the topology of the problem. In the ultimate long-length (low-temperature) limit, the system flows either into the QH critical point or gets localized. The obtained value of the critical conductivity is $\sigma_* \simeq 0.4e^2/h$ times the degeneracy factor (equal to four for scalar impurities). The localization at $E = 0$ takes place when the critical state of the zeroth Landau level is shifted by nonsymmetric disorder, or else, split by intervalley scattering on adatoms. When the magnetic field is so strong that the number of flux quanta exceeds the number of impurities, the conductivity recovers its ballistic value $(4/\pi)e^2/h$.

The work was supported by the EPSRC Doctoral Training Centre in Condensed Matter Physics (S. G.) and the Scottish Universities Physics Alliance (W. R. H.), by the Dutch Science Foundation NWO/FOM Grants No. 13PR3118, by the EU network InterNoM, by DFG SPP No. 1459, and by BMBF. M. T. is grateful to KIT for hospitality.

[1] K. S. Novoselov, A. K. Geim, S. V. Morozov, D. Jiang, Y. Zhang, S. V. Dubonos, I. V. Grigorieva, and A. A. Firsov, Science **306**, 666 (2004); K. S. Novoselov, D. Jiang, T. Booth, V. V. Khotkevich, S. M. Morozov, and A. K. Geim, Proc. Natl. Acad. Sci. U.S.A. **102**, 10451 (2005); A. K. Geim and K. S. Novoselov, Nat. Mater. **6**, 183 (2007); A. K. Geim, Science **324**, 1530 (2009); K. S. Novoselov, Rev. Mod. Phys. **83**, 837 (2011); A. K. Geim, Rev. Mod. Phys. **83**, 851 (2011).

[2] A. H. Castro Neto, F. Guinea, N. M. R. Peres, K. S. Novoselov, and A. K. Geim, Rev. Mod. Phys. **81**, 109 (2009).

[3] D. C. Elias, R. R. Nair, T. M. G. Mohiuddin, S. V. Morozov, P. Blake, M. P. Halsall, A. C. Ferrari, D. W. Boukhvalov, M. I. Katsnelson, A. K. Geim, and K. S. Novoselov, Science **323**, 610 (2009).

[4] S. Ryu, M. Y. Han, J. Maultzsch, T. F. Heinz, P. Kim, M. L. Steigerwald, and L. E. Brus, Nano Lett. **8**, 4597 (2008).

[5] B. R. Matis, F. A. Bulat, A. L. Friedman, B. H. Houston, and J. W. Baldwin, Phys. Rev. B **85**, 195437 (2012); J. S. Burgess, B. R. Matis, J. T. Robinson, F. A. Bulat, F. K. Perkins, B. H. Houston, and J. W. Baldwin, Carbon **49**, 4420 (2011); B. R. Matis, J. S. Burgess, F. A. Bulat, A. L. Friedman, B. H. Houston, and J. W. Baldwin, ACS Nano **6**, 17 (2012).

[6] J. Katoch, J.-H. Chen, R. Tsuchikawa, C. W. Smith, E. R. Mucciolo, and M. Ishigami, Phys. Rev. B **82**, 081417(R) (2010).

[7] J. T. Robinson, J. S. Burgess, C. E. Junkermeier, S. C. Badescu, T. L. Reinecke, F. K. Perkins, M. K. Zalalutdniov, J. W. Baldwin, J. C. Culbertson, P. E. Sheehan, and E. S. Snow, Nano Lett. **10**, 3001 (2010).

[8] F. Schedin, A. K. Geim, S. V. Morozov, E. W. Hill, P. Blake, M. I. Katsnelson, and K. S. Novoselov, Nat. Mater. **6**, 652 (2007).

[9] L. Liu, S. Ryu, M. R. Tomasik, E. Stolyarova, N. Jung, M. S. Hybertsen, M. L. Steigerwald, L. E. Brus, G. W. Flynn, Nano Lett. **8**, 1965 (2008).

[10] J.-H. Chen, W. G. Cullen, C. Jang, M. S. Fuhrer, E. D. Williams, Phys. Rev. Lett. **102**, 236805 (2009).

[11] J.-H. Chen, W. G. Cullen, E. D. Williams, and M. S. Fuhrer, Nat. Phys. **7**, 535 (2011).

[12] D. Teweldebrhan and A. A. Balandin, Appl. Phys. Lett. **94**, 013101 (2009); D. Teweldebrhan and A. A. Balandin, Appl. Phys. Lett. **95**, 246102 (2009); G. Liu, D. Teweldebrhan, and A. A. Balandin, IEEE Trans. Nanotechnol. **10**, 865 (2011).

[13] B. M. Kessler, C. Ö. Girit, A. Zettl, and V. Bouchiat, Phys. Rev. Lett. **104**, 047001 (2010).

[14] T. O. Wehling, A. Balatsky, M. Katsnelson, A. Lichtenstein, K. Scharnberg, and R. Wiesendanger, Phys. Rev. B **75**, 125425 (2007); T. O. Wehling, M. Katsnelson, and A. Lichtenstein, Phys. Rev. B **80**, 085428 (2009); T. O. Wehling, S. Yuan, A. I. Lichtenstein, A. K. Geim, and M. I. Katsnelson, Phys. Rev. Lett. **105**, 056802 (2010).

[15] X. Du, I. Skachko, A. Barker, and E. Y. Andrei, Nat. Nanotechnol. **3**, 491 (2008); X. Du, I. Skachko, and E. Y. Andrei, Int. J. Mod. Phys. B **22**, 4579 (2008); D. A. Abanin, I. Skachko, X. Du, E. Y. Andrei, and L. S. Levitov, Phys. Rev. B **81**, 115410 (2010).

[16] K. I. Bolotin, K. J. Sikes, Z. Jiang, M. Klima, G. Fudenberg, J. Hone, P. Kim, and H. L. Stormer, Solid State Commun. **146**, 351 (2008); K. I. Bolotin, K. J. Sikes, J. Hone, H. L. Stormer, and P. Kim, Phys. Rev. Lett. **101**, 096802 (2008).

[17] P. M. Ostrovsky, I. V. Gornyi, and A. D. Mirlin, Phys. Rev. B **74**, 235443 (2006).

[18] T. Stauber, N. M. R. Peres, and F. Guinea, Phys. Rev. B **76**, 205423 (2007).

[19] D. S. Novikov, Phys. Rev. B **76**, 245435 (2007).

[20] D. M. Basko, Phys. Rev. B **78**, 115432 (2008).

[21] J. P. Robinson, H. Schomerus, L. Oroszlany, and V. I. Falko, Phys. Rev. Lett. **101**, 196803 (2008).

[22] V. M. Pereira, J. M. B. Lopes dos Santos, and A. H. Castro Neto, Phys. Rev. B **77**, 115109 (2008).

[23] S. Yuan, H. De Raedt, and M. I. Katsnelson, Phys. Rev. B **82**, 115448 (2010).

[24] K. S. Novoselov, A. K. Geim, S. V. Morozov, D. Jiang, M. I. Katsnelson, I. V. Grigorieva, S. V. Dubonos, and A. A. Firsov, Nature (London) **438**, 197 (2005).

[25] Y. Zhang, Y.-W. Tan, H. L. Stormer, and P. Kim, Nature (London) **438**, 201 (2005); Y.-W. Tan, Y. Zhang, H. L. Stormer, and P. Kim, Eur. Phys. J. Spec. Top. **148**, 15 (2007).
[26] F. Evers and A. D. Mirlin, Rev. Mod. Phys. **80**, 1355 (2008).
[27] P. M. Ostrovsky, I. V. Gornyi, and A. D. Mirlin, Phys. Rev. Lett. **98**, 256801 (2007); , Eur. Phys. J. Spec. Top. **148**, 63 (2007).
[28] L. A. Ponomarenko, A. K. Geim, A. A. Zhukov, R. Jalil, S. V. Morozov, K. S. Novoselov, V. V. Cheianov, V. I. Fal'ko, K. Watanabe, T. Taniguchi, and R. V. Gorbachev, Nat. Phys. **7**, 958 (2011).
[29] K. S. Novoselov, Z. Jiang, Y. Zhang, S. V. Morozov, H. L. Stormer, U. Zeitler, J. C. Maan, G. S. Boebinger, P. Kim, and A. K. Geim, Science **315**, 1379 (2007).
[30] K. S. Novoselov, A. K. Geim, S. V. Morosov, D. Jiang, M. I. Katsnelson, I. V. Grigorieva, S. V. Dubonos, and A. A. Firsov, Nature (London) **438**, 197 (2005); Y. Zhang, Y.-W. Tan, H. L. Stormer, and P. Kim, Nature (London) **438**, 201 (2005).
[31] D. A. Abanin, K. S. Novoselov, U. Zeitler, P. A. Lee, A. K. Geim, and L. S. Levitov, Phys. Rev. Lett. **98**, 196806 (2007).
[32] J. G. Checkelsky, L. Li, and N. P. Ong, Phys. Rev. Lett. **100**, 206801 (2008); , Phys. Rev. B **79**, 115434 (2009).
[33] Y. Zhao, P. Cadden-Zimansky, F. Ghahari, and P. Kim, Phys. Rev. Lett. **108**, 106804 (2012).
[34] K. I. Bolotin, F. Ghahari, M. D. Shulman, H. L. Stormer, and P. Kim, Nature (London) **462**, 196 (2009).
[35] X. Du, I. Shachko, F. Duerr, A. Luican, and E. Y. Andrei, Nature (London) **462**, 192 (2009).
[36] P. M. Ostrovsky, I. V. Gornyi, and A. D. Mirlin, Phys. Rev. B **77**, 195430 (2008).
[37] A. Lherbier, B. Biel, Y.-M. Niquet, and S. Roche, Phys. Rev. Lett. **100**, 036803 (2008); A. Lherbier, Simon M.-M. Dubois, X. Declerck, S. Roche, Y.-M. Niquet, and J.-C. Charlier, Phys. Rev. Lett. **106**, 046803 (2011); N. Leconte, A. Lherbier, F. Varchon, P. Ordejon, S. Roche, and J.-C. Charlier, Phys. Rev. B **84**, 235420 (2011).
[38] A. Cresti, F. Ortmann, T. Louvet, D. Van Tuan, and S. Roche, Phys. Rev. Lett. **110**, 196601 (2013).
[39] G. T. de Laissardiere and D. Mayou, Mod. Phys. Lett. B **25**, 1019 (2011); , Phys. Rev. Lett. **111**, 146601, (2013).
[40] M. Titov, P. M. Ostrovsky, I. V. Gornyi, A. Schuessler, and A. D. Mirlin, Phys. Rev. Lett. **104**, 076802 (2010).
[41] P. M. Ostrovsky, M. Titov, S. Bera, I. V. Gornyi, and A. D. Mirlin, Phys. Rev. Lett. **105**, 266803 (2010).
[42] J. Schelter, P. M. Ostrovsky, I. V. Gornyi, B. Trauzettel, and M. Titov, Phys. Rev. Lett. **106**, 166806 (2011).
[43] J. Tworzydło, B. Trauzettel, M. Titov, A. Rycerz, and C. W. J. Beenakker, Phys. Rev. Lett. **96**, 246802 (2006).
[44] A. Schuessler, P. M. Ostrovsky, I. V. Gornyi, and A. D. Mirlin, Phys. Rev. B **79**, 075405 (2009).
[45] See Supplemental Material at http://link.aps.org/supplemental/10.1103/PhysRevLett.112.026802 for technical details.
[46] F. Ortmann and S. Roche, Phys. Rev. Lett. **110**, 086602 (2013).
[47] K. Nomura, S. Ryu, M. Koshino, C. Mudry, and A. Furusaki, Phys. Rev. Lett. **100**, 246806 (2008).
[48] Y. Avishai, M. Ya. Azbel, and S. A. Gredeskul, Phys. Rev. B **48**, 17280 (1993); M. Ya. Azbel, Phys. Rev. B **49**, 5463 (1994); M. Ya. Azbel and B. I. Halperin, Phys. Rev. B **52**, 14098 (1995); S. A. Gredeskul, M. Zusman, Y. Avishai, and M. Ya. Azbel, Phys. Rep. **288**, 223 (1997).